SCIENTIFIC REPORTS
nature research

OPEN

Monodisperse Pt-Co/GO anodes with varying Pt: Co ratios as highly active and stable electrocatalysts for methanol electrooxidation reaction

Hakan Burhan, Hasan Ay, Esra Kuyuldar & Fatih Sen*

The intense demand for alternative energy has led to efforts to find highly efficient and stable electrocatalysts for the methanol oxidation reaction. For this purpose, herein, graphene oxide-based platinum-cobalt nanoparticles ($Pt_{100-x}Co_x$@GO NPs) were synthesized in different ratios and the synthesized nanoparticles were used directly as an efficient electrocatalyst for methanol oxidation reaction (MOR). The characterizations for the determination of particle size and surface composition of nanoparticles were performed by transmission electron microscopy (TEM), X-ray diffraction (XRD) and X-ray photoelectron spectroscopy (XPS). The structure of the catalysts was detected as face-centered cubic and the dispersion of them on graphene oxide was homogenous (distributed narrowly (4.01 ± 0.51 nm)). Cyclic voltammetry (CV) and chronoamperometry (CA) was utilized for testing electrocatalytic activities of all prepared NPs for the methanol oxidation reaction. It was detected that the newly produced NPs were more active and stable than commercially existing Pt(0)/Co nanomaterial in methanol electro-oxidation in acidic media.

The researches for environmentally friendly and reusable power have been enhancing due to the gradually increasing pollution issues of the earth. Fuel cells, which are one of the alternative energy sources, are electrochemical cells that convert chemical energy directly into electrical energy with high conversion efficiency and low environmental pollution. In recent years, several studies have been conducted directly on alcohol fuel cells[1–5]. Direct alcohol fuel cells (DAFCs) are used in portable electronic devices because they are more ergonomic as energy sources. DAFCs have become popular among fuel cells because of their easy supply of alcohol derivatives, high energy densities, and relatively easy storage and transport processes. Among the direct alcohol fuel cells, direct methanol fuel cells (DMFCs) are among the most widely studied alcohol fuel types. Because methanol has a structurally simple, easily available and promising electrochemical activity. Due to these properties, many studies have been carried out on electrooxidation[6–8]. Besides, methanol has many advantageous over pure hydrogen as fuel, such as transportability, storage, cost-effectiveness and high theoretical energy density[9–11]. As in all fuel cells, the reaction mechanisms of alcohol with a catalyst that affect the efficiency of these mechanisms are one of the most important parameters in alcohol fuel cells. So far, many studies have been carried out on these catalysts[12–14]. Some of the main problems in the application of DMFCs can be listed as follows: Poisoning caused by adsorption of CO and similar intermediates formed during dehydrogenation of the methanol by catalysts (eg platinum and platinum-based catalysts). This poisoning reduces the efficiency of methanol oxidation kinetics by inhibiting the operation of active sites of catalysts. Another problem is that the platinum catalysts used are very expensive to be commercially available, as the fuel cells show superior performance in the anode section. In order to make it commercially viable, platinum was modified with different metals and more economical alloys or mixtures[15–26]. The catalytic activity and stability of the present electrocatalysts are not efficient enough to directly commercialize methanol fuel cells and make them widely available[7,27,28]. Within these catalysts, Pt+second metal bimetallic nanoparticles bonded onto the graphene oxide support were considered to be one of the most attractive

Sen Research Group, Biochemistry Department, Faculty of Arts and Science, Dumlupınar University, Evliya Çelebi Campus, 43100, Kütahya, Turkey. *email: fatih.sen@dpu.edu.tr

electrocatalysts for the methanol electro-oxidation reaction as a direct anodic reaction of methanol fuel cells[29,30]. Therefore, various studies have been conducted to investigate bimetallic catalysts such as PtSn[31,32], PtPb[33], PtNi[34], PtAu[35,36], PtMo[37]. Catalytic performance and utilization efficiency may vary greatly depending on the performance of the platinum-based electrocatalyst in the fuel cell depending upon the type of support and metals[38–40]. Supporting and/or stabilizing agents are also very important materials in catalytic systems. They result in increasing dispersity, electron transfer, long-term stability and transport of materials in fuel cell electrodes. Nowadays, many scientists have been much interested in graphene and graphene-based supports[41–43]. In this context, various studies have been made by using Platinum-based NPs with graphene due to the very good electrical conduction and good performance of graphene[44–47]. Because graphene oxide (GO) and graphene-based materials are highly dispersible in H_2O and a few organic solvents[48–53]. Over the years many PtCo catalysts with various ratios and morphology has been reported for catalyzing the electrooxidation of methanol[54–56]. For this purpose, in our laboratory, many studies have been carried out in order to increase the efficiency of the catalyst with the help of the addition of second metal and using of different supporting agent[53,57]. In this context, herein, GO-supported platinum-cobalt NPs were synthesized in various ratios by using the double solvent reduction method in this work. All prepared catalysts have been characterized by XRD, XPS, TEM, HR-TEM etc. in order to reveal the morphology and structure of the prepared catalysts. Further, they have been tested for their electrocatalytic efficiency towards methanol oxidation reactions.

Experimental

The chemicals, instruments and the experimental details are given in supporting information. Graphene powder from graphite powder (GO) was synthesized using the Hummer's method[58,59]. All prepared $Pt_{100-x}Co_x$@GO NPs were synthesized by a double solvent reduction method. In shortly, for the preparation of NPs with a various atomic ratio of Pt and Co (1:0, 1:1, 1:3, 3:1 ratio), the calculated amount of $PtCl_4$ and $CoCl_2$ as precursor materials were dissolved in tetrahydrofuran to be able to prepare the NPs and then. The prepared GO was added to the medium as stabilizing and supporting agents with a 1:1 ratio of platinum-cobalt nanoparticles. Ethanol and super hydride ($Li(C_2H_5)_3BH$) were added up to the complete reduction of Pt and Co metals. The formation of $Pt_{100-x}Co_x$ NPs is understood by the observation of brown-black color in solution. Finally, the resulting solid $Pt_{100-x}Co_x$ NPs were dried under a vacuum.

Results and Discussion

All prepared catalysts were characterized by XRD, XPS, TEM, and RAMAN spectroscopy methods. XRD (X-ray diffraction) was used to determine the size of the crystallites and the crystalline structure of the prepared catalysts. In all XRD patterns, Pt (111), Pt (200), Pt (220) and Pt (311) diffraction peaks were clearly shown as an indication of the faced-centered cubic (fcc) structure of the prepared NPs. Besides, the peak at 26° corresponds to C (002) plane which indicates the existence of GO. As shown in Fig. 1a, there are four diffraction peaks at values of 40.1°, 46.3°, 67.4° and 81.4°, which are related to (111), (200), (220) and (311), respectively (Fig. 1a) (JCPDS 87–0646). Specifically, the Pt (111) peak shifts from 39.9 ° (pure Pt) to 40.13 °, 40.21 °, and 40.30 °, for $Pt_{75}Co_{25}$@GO, $Pt_{50}Co_{50}$@GO, and $Pt_{25}Co_{75}$@GO, respectively. This case indicates the alloy formation in all prepared bimetallic nanoparticles.

The characteristic plane of Pt (111) shows the crystalline structure of the nanoparticle and a shift of 2θ degree occurs with increasing cobalt concentration. This can be explained by the formation of cage shrinkage due to the integration of cobalt which is a smaller atom than Pt. The average crystallite size was calculated for $Pt_{100-x}Co_x$@GO using Scherrer formula.

$$d(\text{Å}) = \frac{k\lambda}{\beta cos\theta}$$

where;

k = a coefficient (0.9)

λ = the wavelength of X-ray used (1.54056 Å)

β = the full-width half-maximum of respective diffraction peak (rad)

θ = the angle at the position of peak maximum (rad)

A decrease in the lattice parameter is observed as a result of the increase in Co concentration in the PtCo nanocatalyst (Table 1). This is considered to be the case that Co fills the internal spaces between Pt atoms. Raman spectroscopy was also used to visualize the changes after PtCo addition on the GO surface. Figure 1b shows the values of the D and G bands related to GO, Pt@GO and PtCo@GO. As shown in this figure, here, the G band shows the E_{2g} construction mode of the carbon atoms bound to sp^2, while the D band shows the A_{1g} breathing mode of an irregular graphite structure. The ratios of D-and G-band (I_D/I_G) intensities for GO, Pt@GO, and $Pt_{75}Co_{25}$@GO were 1.10, 1.25, and 1.32, respectively. The increasing ratio of D/G band means the functionalization and/or increasing irregularity of the graphene oxide surface after the addition of PtCo NPs. The size, composition, and morphology of $Pt_{75}Co_{25}$@GO NPs are shown in Fig. 2 as a model catalyst. The morphology of the prepared catalyst is also shown in Fig. 2b with a high-resolution electron micrograph (HRTEM). From the HRTEM image, it can be said that the particles are generally spherical and do not agglomerate in the synthesized catalyst. Furthermore, the atomic lattice fringes are seen by the HRTEM image of the monodisperse $Pt_{75}Co_{25}$ NPs as shown in Fig. 2b. As a result of these fringes, a Pt (111) plane was observed on the prepared catalyst in a range of 0.22 nm; which is similar to a nominal Pt (111) range of 0.23 nm. In addition, the mean particle size of $Pt_{75}Co_{25}$@GO NPs was found to be 4.01 ± 0.51 nm (Fig. 2c) which is in good agreement with XRD results. Further, TEM-EELS mapping of $Pt_{75}Co_{25}$@GO NPs was also performed in order to see the structure of the catalyst and it's seen that Pt and Co co-exist together which also confirms the alloy formation of prepared catalyst. In

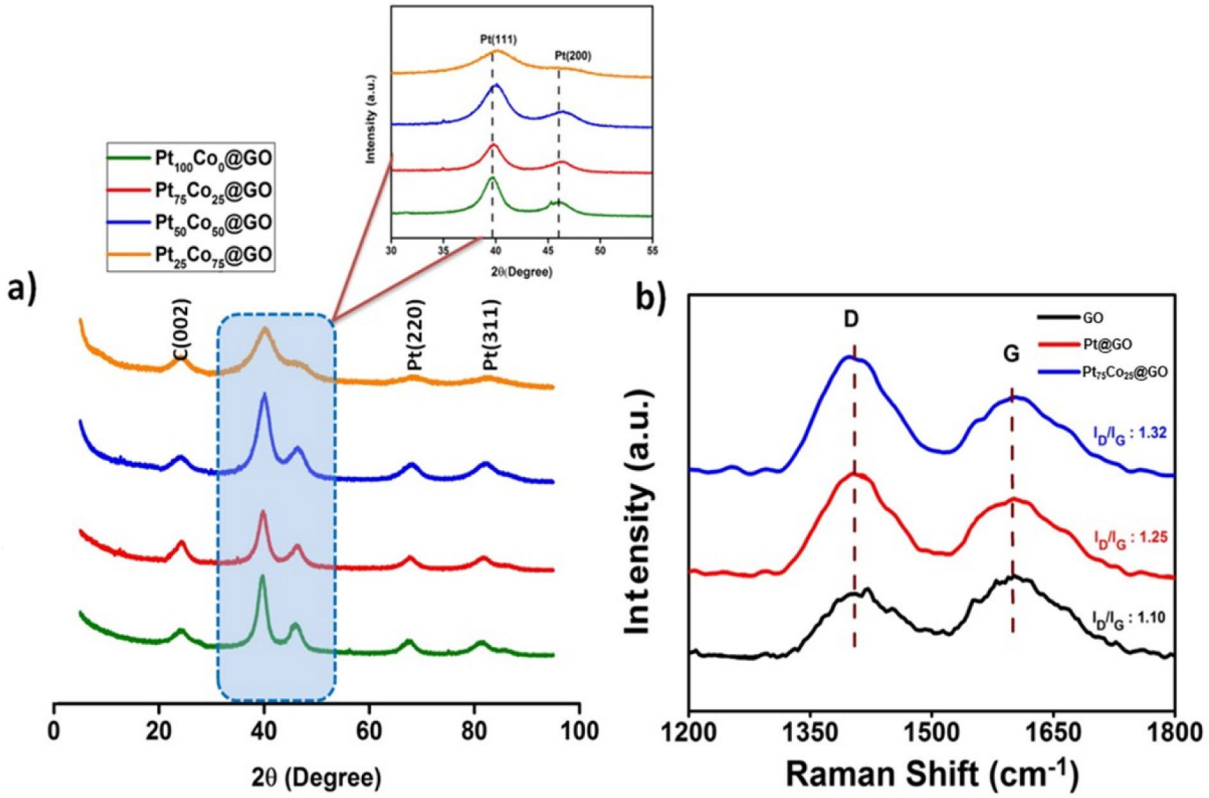

Figure 1. X-ray diffraction (XRD) patterns for all prepared $Pt_{100-x}Co_x$@GO catalysts (**a**), Raman spectra of GO, Pt@GO, and $Pt_{75}Co_{25}$@GO as a model catalyst (**b**).

	a (nm)	b (nm)
$Pt_{100}Co_0$@GO	~4.45	~4.30
$Pt_{75}Co_{25}$@GO	~3.87	~4.01
$Pt_{50}Co_{50}$@GO	~3.66	~3.52
$Pt_{25}Co_{75}$@GO	~3.48	~3.21

Table 1. The comparison of particle size obtained from (a) XRD, (b) TEM.

addition, the formation of an alloy composition with uniformly distributed platinum and cobalt throughout the entire nanoparticle was shown in this figure.

The surface composition and chemical oxidation states of Pt and Co in monodisperse $Pt_{100-x}Co_x$@GO NPs were investigated using X-ray photoelectron spectroscopy (XPS). As a result of this, the Pt 4 f and Co 2p regions of the spectrum were evaluated by the Gaussian-Lorentzian method and the relative density of the species was estimated by calculating the integral of each peak after Shirley background subtraction. The correct binding energies (± 0.3 eV) in the shaped background XPS spectrum were determined with reference to the C1s peak at 284.5 eV (Fig. S1). As shown in Fig. 3, XPS spectra show that the surface Pt and Co are found to be mostly metallic and a small amount of oxides (Fig. 3a,b). Though platinum is mainly metallic form in $Pt_{100-x}Co_x$@GO, from the images, the presence of PtO and PtO_2, indicative of the oxidation of surface was understood from the existence of 2+ and 4+ species. Table S1 represents BEs of the $4f_{7/2}$ data for $Pt_{100-x}Co_x$@GO and Pt@GO and their comparative densities. It is illustrated in Table S1 that the highest amount of platinum (0) is shown in $Pt_{75}Co_{25}$@GO compared to all other prepared ones. From Table S1 and Fig. 3a,b, binding energy (for $4f_{7/2}$ peak) of platinum cobalt/graphene-oxide nanomaterials is 0.1–0.2 eV higher comparing to bulk platinum ones. The cause of positive change is the interaction between the final state of relaxation and platinum/cobalt-graphene-oxide. Table S1 also shows the relative intensities of metallic species in all prepared catalysts and the higher platinum (0) content (83.1%) was shown in $Pt_{75}Co_{25}$@GO compared to the other prepared $Pt_{100-x}Co_x$@GO. When Co 2p peaks are examined, it's seen that cobalt is in mostly zero oxidation state at about 780 eV and in a small amount of oxidized species at about 786 eV.

After full characterization of prepared catalysts, the electrocatalytic performance of $Pt_{100-x}Co_x$@GO was employed towards methanol oxidation reaction. For this purpose, the prepared electrodes with the help of nanomaterials were dipped into 0.5 M sulfuric acid in order to prepare electrocatalyst for the measurements. To obtain

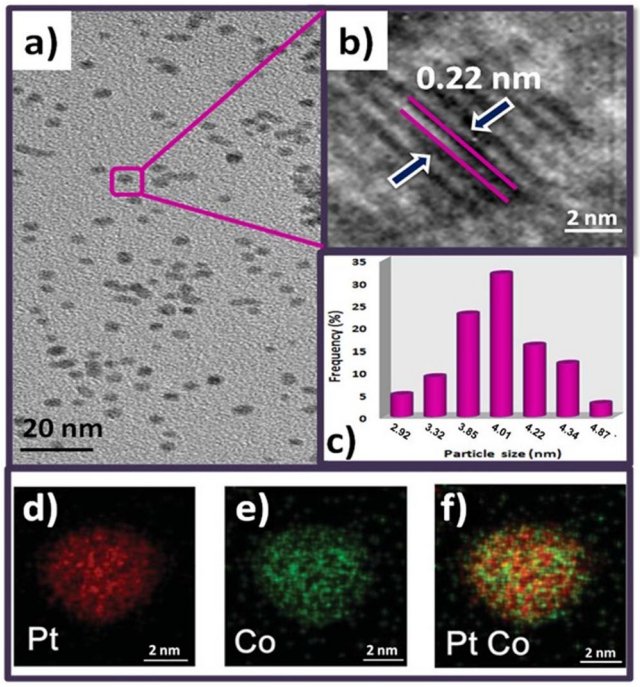

Figure 2. TEM (**a**) and HR-TEM (**b**) images of $Pt_{75}Co_{25}$@GO NPs with particle size histogram (**c**) EELS elemental mapping of $Pt_{100}Co_0$, Pt_0Co_{100}, and $Pt_{75}Co_{25}$ nanocomposites, respectively (**d–f**).

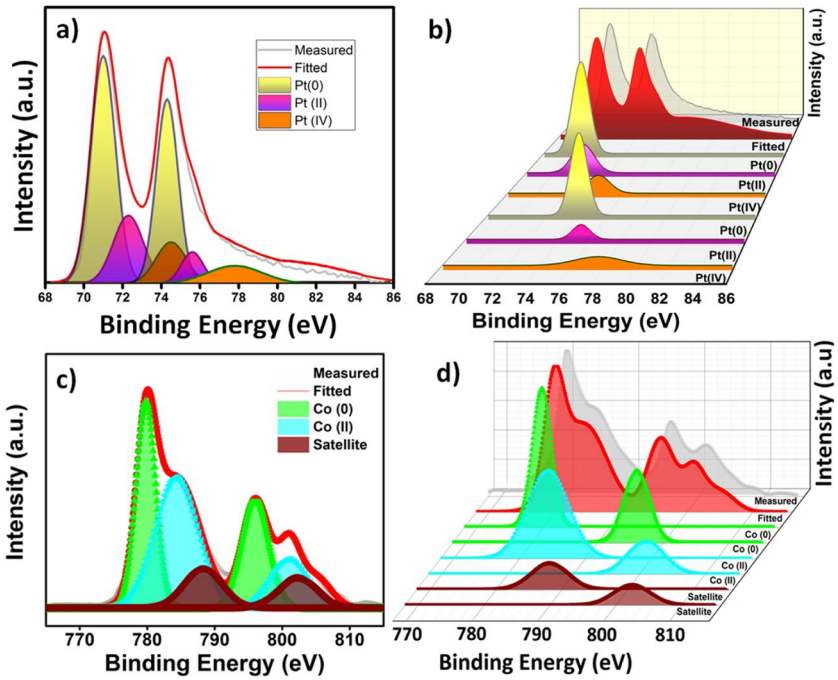

Figure 3. The Pt 4 f (**a,b**) and Co 2p (**c,d**) XPS spectra of $Pt_{75}Co_{25}$@GO NPs.

consistent results in cyclic voltammetry (CV), electrodes were processed among −0.2 and 0.8 V at 50 mV s^{-1}. The cyclic voltammograms of all prepared $Pt_{25}Co_{75}$@GO, $Pt_{50}Co_{50}$@GO, $Pt_{100}Co_0$@GO and $Pt_{75}Co_{25}$@GO electrodes are illustrated in Fig. 4a. A strong oxidation peak is observed in all prepared catalysts. It is also seen from Fig. 4a that the methanol oxidation peak is situated at about 0.38 V for $Pt_{75}Co_{25}$@GO. As shown in Fig. 4a, the best catalytic performance was seen in $Pt_{75}Co_{25}$@GO electrodes which have 1.27, 1.44, 1.54 and 2.94 higher performance than $Pt_{100}Co_0$@GO, $Pt_{50}Co_{50}$@GO, PtRu (20%) E-TEK, and $Pt_{25}Co_{75}$@GO catalysts, respectively. The prepared best catalyst have also been compared with PtRu (ETEK), PtCo@C, PtCo@GC and it was seen that $Pt_{75}Co_{25}$@GO showed better catalytic performance compared to the others as shown in Fig. S2 and S3.

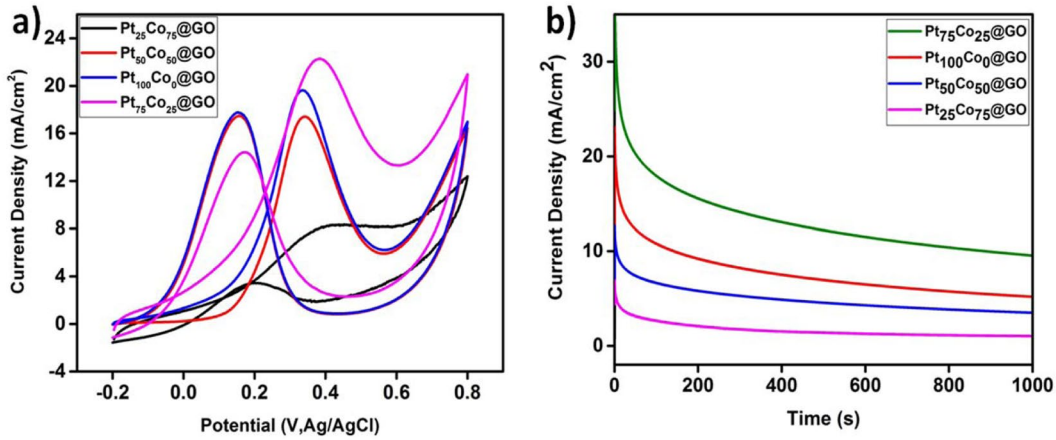

Figure 4. CV reaction profiles during methanol electro-oxidation of the $Pt_{100-x}Co_x$@GO catalysts performed in a 0.5 M CH_3OH + 0.5 M H_2SO_4 solution saturated with N_2 at 25 °C at a scan rate of 50 mV/s (**a**), CA reaction profiles during methanol electro-oxidation of the $Pt_{100-x}Co_x$@GO catalysts in an 0.5 M CH_3OH + 0.5 M H_2SO_4 solution saturated with N_2 at 25 °C (**b**) (0.4 V). cm^2.

In order to explain the higher performance of $Pt_{75}Co_{25}$@GO electrodes, electrochemical surface area (ECSA), chemical surface area (CSA) and metal utility % (ECSA/CSA) were calculated as shown in Table S2. In this table, the comparison of crystalline particle size, ECSA, CSA and metal utilization (%) for the prepared catalysts are given in detail[60]. These data show that $Pt_{75}Co_{25}$@GO NPs have the highest metal utility (89.38%) compared to the other prepared ones. This case explains very well the higher performance of $Pt_{75}Co_{25}$@GO NPs than the other prepared ones. In addition, higher methanol oxidation reaction performance of $Pt_{75}Co_{25}$@GO NPs can be explained by several ways correlating with XPS, TEM, etc. X-ray photoelectron spectroscopy data in Table S1 reveals that platinum is in the more metallic state in $Pt_{75}Co_{25}$@GO NPs (83.1%) than the other prepared ones and consequently causes a more effective activation of adsorbed CH_3OH. The higher performance of $Pt_{100-x}Co_x$@GO is achieved when the more metallic state of platinum is observed in the catalyst because of mixing with cobalt. Besides, the great NPs distribution on graphene oxide leads to an extensive increase in the catalytic performance of $Pt_{100-x}Co_x$@GO and is also the demonstration of the positive impact of utilizing graphene oxide. When all prepared catalysts were compared, $Pt_{75}Co_{25}$@GO NPs exhibited higher performance catalytically in the methanol oxidation reaction, that's why the examination to reveal long-time stability was performed by using 0.5 M methanol and 0.5 M sulfuric acid mixture by chronoamperometry (CA) as shown in Fig. 4b. It can be concluded from the figure (Fig. 4b) that for all catalysts, the peak currents decrease during the time. However, after 3600 seconds, $Pt_{75}Co_{25}$@GO NPs have still higher catalytic activity and stability compared to the other prepared $Pt_{100-x}Co_x$@GO ones. Catalytic lifetime measurements of $Pt_{75}Co_{25}$@GO NPs (the best catalyst in prepared ones) are performed in a nitrogen saturated solution of 0.5 M H_2SO_4 containing 0.5 M CH_3OH at a scan rate of 50 mV s^{-1} at a 1st and 1000th cycle (vs. Ag/AgCl). As shown in Fig. S4, when it's compared to the current between the 1st and 1000th cycle, it can be said that there is only a 12.48% decrease of the initial performance of $Pt_{75}Co_{25}$@GO NPs which shows the high stability and durability of the current catalyst. It is important to investigate the high efficiency and stability of Pt-based electrocatalysts. However, it has been found that small Pt nanoparticles can easily be separated from carbon supports and their stability is discussed[21]. Stability problems in PtRu-based catalysts which are considered active catalysts for MOR activity prevent commercial use[61]. Therefore, studies are carried out to protect the catalytic stability at variable molar concentrations and the stability problem is avoided[62]. Similarly, the stability of the $Pt_{75}Co_{25}$@GO NPs, in this study is much better than catalysts formed with other molar concentrations. The $Pt_{75}Co_{25}$@GO NPs displayed good reactivity in the potential (−0.2 V to 0.8 V) with various scan rates from 50 to 250 mV/s (Fig. S5). In addition, electrical conductivity was determined by performing EIS analysis of the support material (Fig. S6). The increase in the current density with the increase in the potential scan rate is attributed to the excitation signal caused during the charging of the interface capacitance by the charge transfer process. Besides, cyclic voltammetry results showed that when the scan rate was increased, the peaks didn't change which shows the very good electrochemical reversibility and high rate performance. Furthermore, the prepared anodic material indicates high current density and capacitance depending upon its morphology and good conductivity.

Conclusions

As a conclusion, the synthesis and characterization of graphene oxide supported platinum-cobalt nanoparticles with different ratios ($Pt_{100-x}Co_x$@GO NPs) were performed. The simple double solvent reduction method was employed to produce NPs as a facile method. The structure of the catalysts was detected as face-centered cubic and the dispersion of them on graphene oxide was homogenous (distributed narrowly (4.01 ± 0.51 nm)). The altered promoter served quite dispersed metal holding parts for the nucleation of NPs on the graphene oxide's surface, allowing a monodisperse and homogeneous distribution of $Pt_{100-x}Co_x$@GO NPs. The synthesized nanoparticles were used directly as anode material in direct methanol fuel cells (DMFCs). Cyclic voltammetry (CV) and chronoamperometry (CA) was utilized for testing electrocatalytic activities of all prepared NPs for

the methanol oxidation reaction. The best catalytic performance was seen in $Pt_{75}Co_{25}$@GO electrodes which have 1.27, 1.44, 1.54 and 2.94 higher performance than $Pt_{100}Co_0$@GO, $Pt_{50}Co_{50}$@GO, PtRu (20%) E-TEK, and $Pt_{25}Co_{75}$@GO catalysts, respectively. Further, $Pt_{75}Co_{25}$@GO NPs have the highest metal utility (89.38%) compared to the other prepared ones. Besides, platinum is in the more metallic state in $Pt_{75}Co_{25}$@GO NPs (83.1%) than the other prepared ones and consequently causes a more effective activation of adsorbed CH_3OH. The higher performance of $Pt_{100-x}Co_x$@GO is achieved when the more metallic state of platinum is observed in the catalyst because of mixing with cobalt. Moreover, there is only a 12.48% decrease in the initial performance of $Pt_{75}Co_{25}$@GO NPs which shows the high stability and durability of the current catalyst. Besides, cyclic voltammetry results showed that when the scan rate was increased, the peaks didn't change which shows the very good electrochemical reversibility and high rate performance. Furthermore, the prepared anodic material indicates high current density and capacitance depending upon its morphology and good conductivity. We believe that $Pt_{75}Co_{25}$@GO NPs will be strategically used in future studies to be used in methanol oxidation reactions. In the near future, these types of materials can also be used in various applications due to their superior properties.

Received: 25 September 2019; Accepted: 27 March 2020;
Published online: 09 April 2020

References

1. Zhang, J. PEM Fuel Cell Electrocatalysts and Catalyst Layers. PEM Fuel Cell Electrocatalysts and Catalyst Layers: Fundamentals and Applications https://doi.org/10.1007/978-1-84800-936-3. (Springer London, 2008).
2. Gu, Y.-J. & Wong, W.-T. Nanostructure PtRu/MWNTs as Anode Catalysts Prepared in a Vacuum for Direct Methanol Oxidation. *Langmuir* **22**, 11447–11452 (2006).
3. Ertan, S., Şen, F., Şen, S. & Gökağaç, G. Platinum nanocatalysts prepared with different surfactants for C1-C3 alcohol oxidations and their surface morphologies by AFM. *J. Nanoparticle Res*. https://doi.org/10.1007/s11051-012-0922-5 (2012).
4. Antolini, E., Salgado, J. R. C. & Gonzalez, E. R. The methanol oxidation reaction on platinum alloys with the first row transition metals. *Appl. Catal. B Environ.* **63**, 137–149 (2006).
5. Yang, H., Zhang, J., Sun, K., Zou, S. & Fang, J. Enhancing by Weakening: Electrooxidation of Methanol on Pt3Co and Pt Nanocubes. *Angew. Chemie Int. Ed.* **49**, 6848–6851 (2010).
6. Şen, S., Şen, F. & Gökağaç, G. Preparation and characterization of nano-sized Pt-Ru/C catalysts and their superior catalytic activities for methanol and ethanol oxidation. *Phys. Chem. Chem. Phys*. https://doi.org/10.1039/c1cp20064j (2011).
7. Şen, F. & Gökağaç, G. Improving catalytic efficiency in the methanol oxidation reaction by inserting Ru in face-centered cubic Pt nanoparticles prepared by a new surfactant, tert-octanethiol. *Energy and Fuels* https://doi.org/10.1021/ef700575t (2008).
8. Yıldız, Y. *et al*. Different ligand based monodispersed Pt nanoparticles decorated with rGO as highly active and reusable catalysts for the methanol oxidation. *Int. J. Hydrogen Energy* https://doi.org/10.1016/j.ijhydene.2017.03.230 (2017).
9. Papadimitriou, S. *et al*. Methanol Oxidation at Pt−Cu, Pt−Ni, and Pt−Co Electrode Coatings Prepared by a Galvanic Replacement Process. *J. Phys. Chem. C* **114**, 5217–5223 (2010).
10. Sen, F., Karatas, Y., Gulcan, M. & Zahmakiran, M. Amylamine stabilized platinum(0) nanoparticles: Active and reusable nanocatalyst in the room temperature dehydrogenation of dimethylamine-borane. *RSC Adv*. https://doi.org/10.1039/c3ra43701a (2014).
11. Liu, L., Pippel, E., Scholz, R. & Gösele, U. Nanoporous Pt−Co Alloy Nanowires: Fabrication, Characterization, and Electrocatalytic Properties. *Nano Lett.* **9**, 4352–4358 (2009).
12. Çelik, B. *et al*. Monodisperse Pt(0)/DPA@GO nanoparticles as highly active catalysts for alcohol oxidation and dehydrogenation of DMAB. *Int. J. Hydrogen Energy* **41**, 5661–5669 (2016).
13. Vigier, F., Rousseau, S., Coutanceau, C., Leger, J.-M. & Lamy, C. Electrocatalysis for the direct alcohol fuel cell. *Top. Catal.* **40**, 111–121 (2006).
14. Yang, Z., Shi, Y., Wang, X., Zhang, G. & Cui, P. Boron as a superior activator for Pt anode catalyst in direct alcohol fuel cell. *J. Power Sources* **431**, 125–134 (2019).
15. Antolini, E., Salgado, J. R. C. & Gonzalez, E. R. The stability of Pt–M (M=first row transition metal) alloy catalysts and its effect on the activity in low temperature fuel cells. *J. Power Sources* **160**, 957–968 (2006).
16. Hyeon, T., Han, S., Sung, Y.-E., Park, K.-W. & Kim, Y.-W. High-Performance Direct Methanol Fuel Cell Electrodes using Solid-Phase-Synthesized Carbon Nanocoils. *Angew. Chemie Int. Ed.* **42**, 4352–4356 (2003).
17. Mu, Y., Liang, H., Hu, J., Jiang, L. & Wan, L. Controllable Pt Nanoparticle Deposition on Carbon Nanotubes as an Anode Catalyst for Direct Methanol Fuel Cells. *J. Phys. Chem. B* **109**, 22212–22216 (2005).
18. Şen, F., Gökağaç, G. & Şen, S. High performance Pt nanoparticles prepared by new surfactants for C 1 to C3 alcohol oxidation reactions. *J. Nanoparticle Res*. https://doi.org/10.1007/s11051-013-1979-5 (2013).
19. Qi, J., Yan, S., Jiang, Q., Liu, Y. & Sun, G. Improving the activity and stability of a Pt/C electrocatalyst for direct methanol fuel cells. *Carbon N. Y.* **48**, 163–169 (2010).
20. Erken, E., Esirden, I., Kaya, M. & Sen, F. A rapid and novel method for the synthesis of 5-substituted 1H-tetrazole catalyzed by exceptional reusable monodisperse Pt NPs@AC under the microwave irradiation. *RSC Adv*. https://doi.org/10.1039/c5ra11426h (2015).
21. Li, C. *et al*. Emerging Pt-based electrocatalysts with highly open nanoarchitectures for boosting oxygen reduction reaction. *Nano Today* **21**, 91–105 (2018).
22. Li, C. *et al*. Electrochemical Deposition: An Advanced Approach for Templated Synthesis of Nanoporous Metal Architectures. *Acc. Chem. Res.* **51**, 1764–1773 (2018).
23. Ataee-Esfahani, H. *et al*. Mesoporous Metallic Cells: Design of Uniformly Sized Hollow Mesoporous Pt-Ru Particles with Tunable Shell Thicknesses. *Small* **9**, 1047–1051 (2013).
24. Li, C. *et al*. Pore-tuning to boost the electrocatalytic activity of polymeric micelle-templated mesoporous Pd nanoparticles. *Chem. Sci.* **10**, 4054–4061 (2019).
25. Ataee-Esfahani, H., Wang, L. & Yamauchi, Y. Block copolymer assisted synthesis of bimetallic colloids with Au core and nanodendritic Pt shell. *Chem. Commun.* **46**, 3684 (2010).
26. Kuyuldar, E. *et al*. Enhanced Electrocatalytic Activity and Durability of PtRu Nanoparticles Decorated on rGO Material for Ethanol Oxidation Reaction. In *Graphene Functionalization Strategies* 389–398 https://doi.org/10.1007/978-981-32-9057-0_16 (2019).
27. Yang, W., Wang, X., Yang, F., Yang, C. & Yang, X. Carbon Nanotubes Decorated with Pt Nanocubes by a Noncovalent Functionalization Method and Their Role in Oxygen Reduction. *Adv. Mater.* **20**, 2579–2587 (2008).
28. Saha, M. S. & Kundu, A. Functionalizing carbon nanotubes for proton exchange membrane fuel cells electrode. *J. Power Sources* **195**, 6255–6261 (2010).
29. Zeng, J. & Yanglee, J. Ruthenium-free, carbon-supported cobalt and tungsten containing binary & ternary Pt catalysts for the anodes of direct methanol fuel cells. *Int. J. Hydrogen Energy* **32**, 4389–4396 (2007).

30. Wang, Z.-C., Ma, Z.-M. & Li, H.-L. Functional multi-walled carbon nanotube/polysiloxane composite films as supports of PtNi alloy nanoparticles for methanol electro-oxidation. *Appl. Surf. Sci.* **254**, 6521–6526 (2008).
31. Karousis, N., Tagmatarchis, N. & Tasis, D. Current Progress on the Chemical Modification of Carbon Nanotubes. *Chem. Rev.* **110**, 5366–5397 (2010).
32. Selvaraj, V., Alagar, M. & Kumar, K. Synthesis and characterization of metal nanoparticles-decorated PPY–CNT composite and their electrocatalytic oxidation of formic acid and formaldehyde for fuel cell applications. *Appl. Catal. B Environ.* **75**, 129–138 (2007).
33. Peng, X. & Wong, S. S. Functional Covalent Chemistry of Carbon Nanotube Surfaces. *Adv. Mater.* **21**, 625–642 (2009).
34. Yue, B. *et al*. CNx nanotubes as catalyst support to immobilize platinum nanoparticles for methanol oxidation. *J. Mater. Chem.* **18**, 1747 (2008).
35. Jiang, S. *et al*. Facile Construction of Pt-Co/CN x Nanotube Electrocatalysts and Their Application to the Oxygen Reduction Reaction. *Adv. Mater.* **21**, 4953–4956 (2009).
36. Ahmadi, R. & Amini, M. K. Synthesis and characterization of Pt nanoparticles on sulfur-modified carbon nanotubes for methanol oxidation. *Int. J. Hydrogen Energy* **36**, 7275–7283 (2011).
37. Bezerra, C. W. B. *et al*. A review of heat-treatment effects on activity and stability of PEM fuel cell catalysts for oxygen reduction reaction. *J. Power Sources* **173**, 891–908 (2007).
38. Liu, Z., Yu, C., Rusakova, I. A., Huang, D. & Strasser, P. Synthesis of Pt3Co Alloy Nanocatalyst via Reverse Micelle for Oxygen Reduction Reaction in PEMFCs. *Top. Catal.* **49**, 241–250 (2008).
39. Schulenburg, H. *et al*. Heat-Treated PtCo 3 Nanoparticles as Oxygen Reduction Catalysts. *J. Phys. Chem. C* **113**, 4069–4077 (2009).
40. Wang, C. *et al*. Monodisperse Pt3Co nanoparticles as electrocatalyst: the effects of particle size and pretreatment on electrocatalytic reduction of oxygen. *Phys. Chem. Chem. Phys.* **12**, 6933 (2010).
41. Wei, Q., Liu, T., Wang, Y. & Dai, L. Three-dimensional N-doped graphene aerogel-supported Pd nanoparticles as efficient catalysts for solvent-free oxidation of benzyl alcohol. *RSC Adv.* **9**, 9620–9628 (2019).
42. Liu, J., Ma, Q., Huang, Z., Liu, G. & Zhang, H. Recent Progress in Graphene-Based Noble-Metal Nanocomposites for Electrocatalytic Applications. *Adv. Mater.* **31**, 1800696 (2019).
43. Demirkan, B. *et al*. Composites of Bimetallic Platinum-Cobalt Alloy Nanoparticles and Reduced Graphene Oxide for Electrochemical Determination of Ascorbic Acid, Dopamine, and Uric Acid. *Sci. Rep.* **9**, 12258 (2019).
44. Watanabe, M. Activity and Stability of Ordered and Disordered Co-Pt Alloys for Phosphoric Acid Fuel Cells. *J. Electrochem. Soc.* **141**, 2659 (1994).
45. Pearson, W. B. & Vineyard, G. H. A Handbook of Lattice Spacings and Structures of Metals and Alloys. *Phys. Today* **11**, 36–36 (1958).
46. Hernández-Fernández, P. *et al*. An opening route to the design of cathode materials for fuel cells based on PtCo nanoparticles. *Appl. Catal. B Environ.* **77**, 19–28 (2007).
47. Miller, J. T. & Koningsberger, D. C. The Origin of Sulfur Tolerance in Supported Platinum Catalysts: The Relationship between Structural and Catalytic Properties in Acidic and Alkaline Pt/LTL. *J. Catal.* **162**, 209–219 (1996).
48. Nakamura, T., Ohana, T., Ishihara, M., Hasegawa, M. & Koga, Y. Chemical modification of single-walled carbon nanotubes with sulfur-containing functionalities. *Diam. Relat. Mater.* **16**, 1091–1094 (2007).
49. Liu, J. Fullerene Pipes. *Science (80-.).* **280**, 1253–1256 (1998).
50. Liu, H., Li, W. & Manthiram, A. Factors influencing the electrocatalytic activity of Pd100−×Cox (0≤ × ≤50) nanoalloys for oxygen reduction reaction in fuel cells. *Appl. Catal. B Environ.* **90**, 184–194 (2009).
51. Xiong, L. & Manthiram, A. Effect of Atomic Ordering on the Catalytic Activity of Carbon Supported PtM (M=Fe, Co, Ni, and Cu) Alloys for Oxygen Reduction in PEMFCs. *J. Electrochem. Soc.* **152**, A697 (2005).
52. Jeon, M. K., Zhang, Y. & McGinn, P. J. Effect of reduction conditions on electrocatalytic activity of a ternary PtNiCr/C catalyst for methanol electro-oxidation. *Electrochim. Acta* **54**, 2837–2842 (2009).
53. Lolak, N. *et al*. Composites of Palladium–Nickel Alloy Nanoparticles and Graphene Oxide for the Knoevenagel Condensation of Aldehydes with Malononitrile. *ACS Omega* **4**, 6848–6853 (2019).
54. Liu, H. *et al*. Uniformly dispersed platinum-cobalt alloy nanoparticles with stable compositions on carbon substrates for methanol oxidation reaction. *Sci. Rep.* **7**, 11421 (2017).
55. Baronia, R. *et al*. PtCo/rGO nano-anode catalyst: enhanced power density with reduced methanol crossover in direct methanol fuel cell. *Mater. Renew. Sustain. Energy* **7**, 27 (2018).
56. Baronia, R., Goel, J. & Singhal, S. K. High Methanol Electro-Oxidation Using PtCo/Reduced Graphene Oxide (rGO) Anode Nanocatalysts in Direct Methanol Fuel Cell. *J. Nanosci. Nanotechnol.* **19**, 4315–4322 (2019).
57. Lolak, N. *et al*. Composites of Palladium–Nickel Alloy Nanoparticles and Graphene Oxide for the Knoevenagel Condensation of Aldehydes with Malononitrile. *ACS Omega* **4**, 6848–6853 (2019).
58. Chen, J., Yao, B., Li, C. & Shi, G. An improved Hummers method for eco-friendly synthesis of graphene oxide. *Carbon N. Y.* **64**, 225–229 (2013).
59. Zaaba, N. I. *et al*. Synthesis of Graphene Oxide using Modified Hummers Method: Solvent Influence. *Procedia Eng.* **184**, 469–477 (2017).
60. Trasatti, S. & Petrii, O. A. Real surface area measurements in electrochemistry. *J. Electroanal. Chem.* **327**, 353–376 (1992).
61. Reddy, G. V. *et al*. Ultrafine Pt–Ru bimetallic nanoparticles anchored on reduced graphene oxide sheets as highly active electrocatalysts for methanol oxidation. *Mater. Chem. Front.* **1**, 757–766 (2017).
62. Baronia, R. *et al*. Efficient electro-oxidation of methanol using PtCo nanocatalysts supported reduced graphene oxide matrix as anode for DMFC. *Int. J. Hydrogen Energy* **42**, 10238–10247 (2017).

Acknowledgements

The authors would like to thank DPÜ-BAP (2018–29) for financial support.

Author contributions

F.S. organized all experiments and wrote the manuscript. H.B., H.A. and E.K. performed all experiments and characterizations. They have also drawn the figures.

Competing interests

The authors declare no competing interests.

Additional information

Supplementary information is available for this paper at https://doi.org/10.1038/s41598-020-63247-6.

Correspondence and requests for materials should be addressed to F.S.

Reprints and permissions information is available at www.nature.com/reprints.